



ELSEVIER

Tectonophysics 293 (1998) 69–84

TECTONOPHYSICS

New seismic images of the Cascadia subduction zone from cruise SO108 — ORWELL

Ernst R. Flueh^{a,*}, Michael A. Fisher^b, Joerg Bialas^a, Jonathan R. Childs^b, Dirk Klaeschen^a,
Nina Kukowski^a, Tom Parsons^b, David W. Scholl^{b,d}, Uri ten Brink^c, Anne M. Tréhu^e,
Neus Vidal^a

^a Universität Kiel, GEOMAR, Wischhofstraße 1–3, 24148 Kiel, Germany

^b U.S. Geological Survey, 345 Middlefield Road, Menlo Park, CA 94025, USA

^c U.S. Geological Survey, Woods Hole, MA 02543, USA

^d Stanford University, Stanford, CA 94305, USA

^e Oregon State University, Corvallis, OR 97331, USA

Received 24 November 1997; accepted 20 April 1998

Abstract

In April and May 1996, a geophysical study of the Cascadia continental margin off Oregon and Washington was conducted aboard the German R/V *Sonne*. This cooperative experiment by GEOMAR and the USGS acquired wide-angle reflection and refraction seismic data, using ocean-bottom seismometers (OBS) and hydrophones (OBH), and multichannel seismic reflection (MCS) data. The main goal of this experiment was to investigate the internal structure and associated earthquake hazard of the Cascadia subduction zone and to image the downgoing plate. Coincident MCS and wide-angle profiles along two tracks are presented here. The plate boundary has been imaged precisely beneath the wide accretionary wedge close to shore at ca. 13 km depth. Thus, the downgoing plate dips more shallowly than previously assumed. The dip of the plate changes from 2° to 4° at the eastern boundary of the wedge on the northern profile, where approximately 3 km of sediment is entering the subduction zone. On the southern profile, where the incoming sedimentary section is about 2.2 km thick, the plate dips about 0.5° to 1.5° near the deformation front and increases to 3.5° further landwards. On both profiles, the deformation of the accretionary wedge has produced six ridges on the seafloor, three of which represent active faulting, as indicated by growth folding. The ridges are bordered by landward verging faults which reach as deep as the top of the oceanic basement. Thus the entire incoming sediment package is being accreted. At least two phases of accretion are evident, and the rocks of the older accretionary phase(s) forms the backstop for the younger phase, which started around 1.5 Ma ago. This documents that the 30 to 50 km wide frontal part of the accretionary wedge, which is characterized by landward vergent thrusts, is a Pleistocene feature which was formed in response to the high input of sediment building the fans during glacial periods. Velocities increase quite rapidly within the wedge, both landward and downward. At the toe of the deformation front, velocities are higher than 4.0 km/s, indicating extensive dewatering of deep, oceanic sediment. Further landward, considerable velocity variation is found, which indicates major breaks throughout the accretionary history. © 1998 Elsevier Science B.V. All rights reserved.

Keywords: Cascadia; seismic reflection; seismic refraction; crustal structure; ocean bottom; seismometer; accretionary wedges

* Corresponding author. Fax: +49 (431) 600-2922; E-mail: eflueh@geomar.de

1. Introduction

Cascadia, which includes the Pacific Northwest of the United States and parts of adjacent British Columbia, Canada, is presently undergoing rapid urban growth. This region is subject to a variety of geohazards, including great earthquakes, explosive volcanoes and tsunamis. These hazards are associated with the Cascadia convergent margin along which the offshore Explorer, Juan de Fuca, and Gorda oceanic plates subduct obliquely northeastward beneath the 1000 km long coast that extends southward from Vancouver Island, B.C., to northern California (Fig. 1).

Recent geologic studies indicate that a great earthquake generated within the Cascadia subduction zone could devastate urban areas of the Pacific Northwest. One such earthquake apparently rocked this region as recently as 300 years ago, and much debate has focussed on the seismic potential of this region (e.g. Heaton and Kanamori, 1984; Atwater, 1992; Hyndman and Wang, 1993; Wang et al., 1995; Satake et al., 1996). Little is known about potential earthquake source regions along the interplate decollement. In fact even the geometry of the downgoing Juan de Fuca Plate beneath Oregon and Washington, heretofore, could not be determined because of the paucity of shallow (<30 km) earthquakes.

The ORWELL Project (ORegon and Washington ExpLoration of the Lithosphere — a geophysical experiment) set out to investigate the crustal structure and earthquake hazards of the Cascadia subduction zone beneath Washington and Oregon. Using the R/V *Sonne* during April and May, 1996, we collected seismic reflection and wide-angle refraction data at sea and on land (Flueh and Fisher, 1996).

Using these data and those from the 1995 Washington seismic transect (Luetgert et al., 1995) we can now accurately track the downgoing plate from the trench to its position below the coast, solving a problem that has long vexed seismologists. Additionally, the structure of the Washington margin is revealed in considerable detail. In the present article, we report on two coincident MCS/wide-angle seismic profiles from the Washington margin and their interpretation.

2. Regional background

The Explorer, Juan de Fuca, and Gorda plates are the last remnants of the Farallon Plate, which was almost completely subducted beneath western North America during Mesozoic and Cenozoic time (Engelbretson et al., 1985). These small plates are separated from the Pacific Plate by the Juan de Fuca Ridge system, which is actively spreading (Delaney et al., 1981; Sinton and Detrick, 1992). Young oceanic lithosphere (4–8 Ma) is presently subducting beneath the Cascadia margin at about 4 cm/yr (DeMets et al., 1990), as the ridge migrates northeastward toward the subduction zone. A thick, actively deforming accretionary wedge is forming along the base of the continental slope off Washington.

Despite the young age of the downgoing Juan de Fuca Plate, a thick sedimentary sequence (about 3.5 km at 45°N) is entering the subduction zone. A lower layer consisting of continentally derived turbidites and hemipelagic mud is overlain by Quaternary sediment of the Astoria Fan off Oregon and the Nitinat Fan off Washington (Applegate et al., 1992). These fans include deposits from the Columbia River and the Strait of Juan de Fuca. The result is a rapid seaward growth of the wedge, about 30 to 50 km over the last 2 m.y. (Barnard, 1978).

The active Cascade magmatic arc, which consists of about 20 major andesitic stratovolcanoes and thousands of smaller volcanic vents, extends 1200 km from Meagher Mountain in southern British Columbia to Lassen Peak in northern California, consistent with the subsurface extent of a subducted slab at about 100 km beneath the full length of the arc (Finn, 1990). Most of the accretionary complex lies offshore, except in the Olympic Mountains and near Cape Mendocino, where parts of the wedge extend onshore. The complex is bordered to the east by Paleocene to Early Eocene basement rock collectively called the Siletz Terrane. The western border of the Siletz Terrane has in places been mapped with seismic reflection and magnetic data (Snively, 1987). Geologic mapping in accretionary assemblages of the western Olympic Mountains (Rau, 1975, 1979; Snively et al., 1986, 1989; Snively and Kvenvolden, 1989) and interpretation of seismic profiles on the Vancouver Island margin (Snively and Wagner, 1981; Clowes et al., 1987; Davis and Hyndman, 1989), on the Wash-

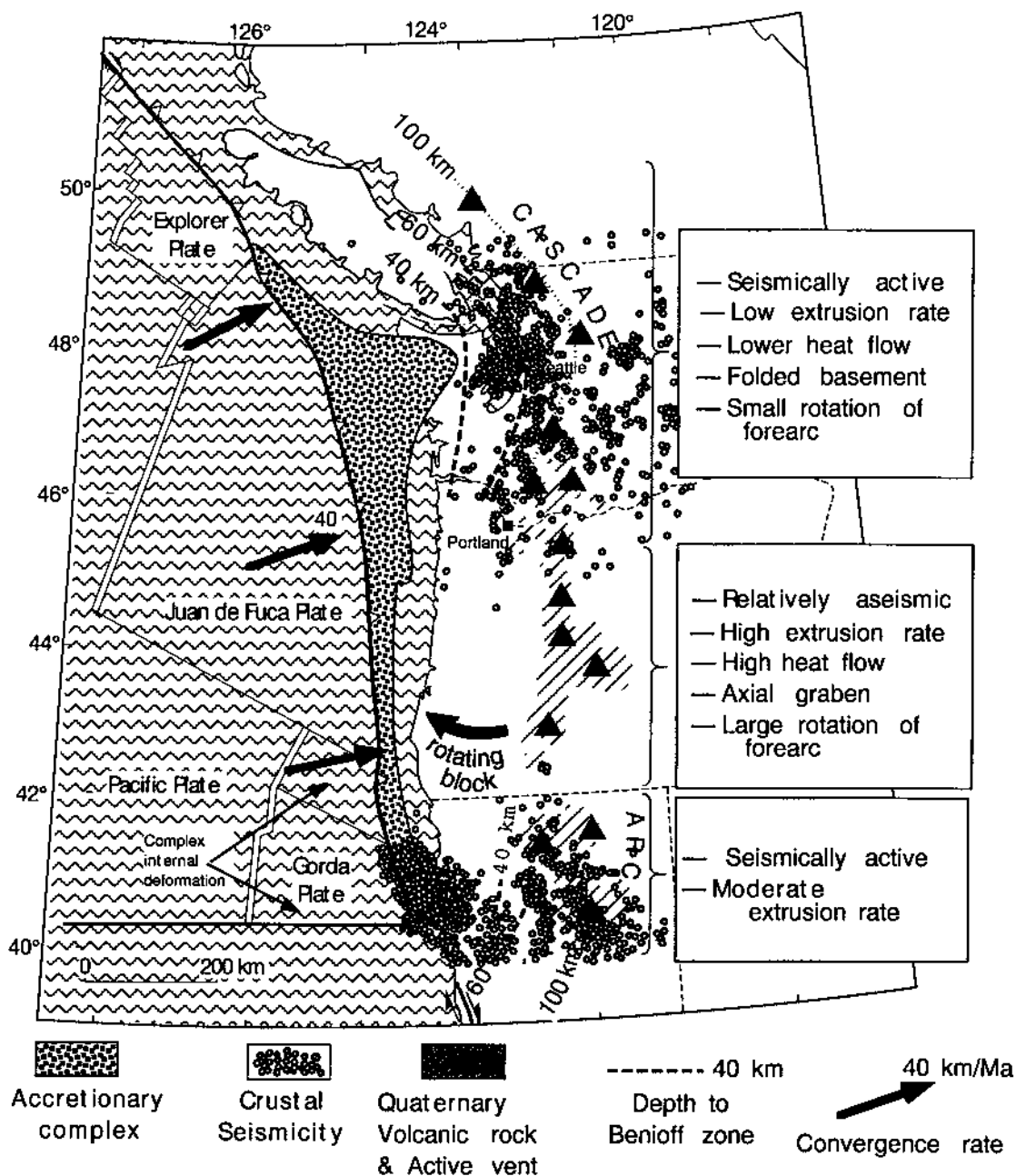


Fig. 1. The main tectonic units and segmentation of the Cascadia margin, modified from Wells et al. (1996).

ington shelf (Snively and Wagner, 1982), and on the Oregon continental slope (Snively et al., 1986, 1987, 1993) indicate that strata as young as Miocene have underplated older rocks along the convergent margin.

In the uplifted core of the Olympic Mountains of northern Washington, accretionary material is thrust beneath the Coast Range basalt basement (Crescent formation) along a major thrust fault that juxtaposes

Middle Eocene melange and broken formation (MBF) to the west against coherent masses of basalt and overlying strata to the east (Tabor and Cady, 1978; Brandon et al., 1988; Snively et al., 1993). On nearby Vancouver Island, reflection and refraction profiles of the Canadian Lithoprobe program indicate that Eocene accretionary strata underplate Lower Eocene basalt and the structurally overlying pre-Tertiary rocks (Clowes et al., 1987; Dragert et al., 1994).

To the south, the extent of the accretionary wedge beneath the rest of the Coast Range is unknown. In a marine multichannel seismic survey and geologic profile across the continental shelf near Grays Harbor, Washington, Snively and Wagner (1982) suggested that part of the accretionary wedge is thrust eastward beneath a thin upper plate of Coast Range basalt. Shelf- and slope-basin fill of Oligocene and younger age overlies the basalt basement offshore. Thrusting, fault-bend folding, and diapiric intrusion of mud matrix melanges continue to deform the accretionary wedge and overlying basin fill to the present. Although the upper levels of the subduction complex have been successfully imaged in several places, the deep structure of the accretionary wedge, its extent beneath the Coast Range basalt, its effect on the geometry of the subducting slab, and its physical properties at depth are poorly understood (Calvert, 1996).

Farther to the south, off central Oregon, the accretionary wedge is narrower, and the Coast Range basalt extends farther offshore (Snively, 1987), possibly forming a backstop for the subduction complex (Snively et al., 1980; Trehu et al., 1994). Most of the seismic profiles off Oregon show an accretionary complex, composed of offscraped sediment and overlying slope basin deposits that are undergoing thrusting and folding from the deformation front landward to a pronounced outer-arc high along the shelf–slope break (e.g. Snively et al., 1980; Niem et al., 1990). In other subduction zones, this outer-arc high typically correlates with the seismic front (Byrne et al., 1988) and presumably the beginning of strong seismic coupling in the subduction zone. However, in Oregon and Washington, there is little or no seismic activity along the coast. According to Byrne et al. (1988), high pore pressure in accretionary wedges inhibits buildup of interplate shear stresses. In support of this observation, over-

pressured melange units have been identified in oil exploration boreholes on the Oregon shelf inboard of the outer-arc high (Snively, 1987).

Although the convergent margin of Cascadia exhibits many characteristics typical of subduction zones, in several ways it is unique because the small subducting oceanic plates offshore Cascadia are caught in the dextral shear couple between the encroaching Pacific and North American plates. The upper (continental) and lower (oceanic) plates thus appear to be breaking up into rotating blocks (Wells and Heller, 1988; Wells, 1989, 1990). As a result, along strike, the Cascadia margin exhibits dramatic north–south variations in seismicity, volcanism, and regional deformational patterns (Fig. 1).

A common feature of the internal structure of submarine accretionary wedges are seaward vergent, imbricate thrust slices separated by landward dipping faults, resulting in sediment accretion and growth of the continental margin (Moore et al., 1990). Off Oregon, however, landward vergence is observed at 45°N while to the north and south, ‘normal’ seaward vergence predominates. This opposite sense of vergence has only occasionally been observed elsewhere. To explain the landward vergence, models have been proposed that apply the Mohr–Coulomb theory, in which low basal shear stress, an arcward dipping decollement and a relatively strong wedge are required (Seely, 1977; MacKay et al., 1992; MacKay, 1995).

2.1. Data acquisition

Geophysical equipment deployed for this experiment included fourteen ocean-bottom hydrophones (OBH) from GEOMAR (Flueh and Bialas, 1996) and nine 3-component ocean-bottom seismometers (OBS) from the USGS. (In this paper we refer to both kinds of instrument as OBS.) A total of 116 deployments was made and processing and plotting of all data as record sections was completed aboard (Flueh and Fisher, 1996). Multichannel seismic (MCS) equipment included a 48-channel, 2400-m streamer that yielded 24-fold, 16-s data. Altogether, thirteen profiles (101 to 113, Fig. 2) with a total length of 1385 km were recorded, and initial processing of two lines was completed while at sea. A critical component of the seismic operation was the airgun array, which consisted of two linear subarrays,

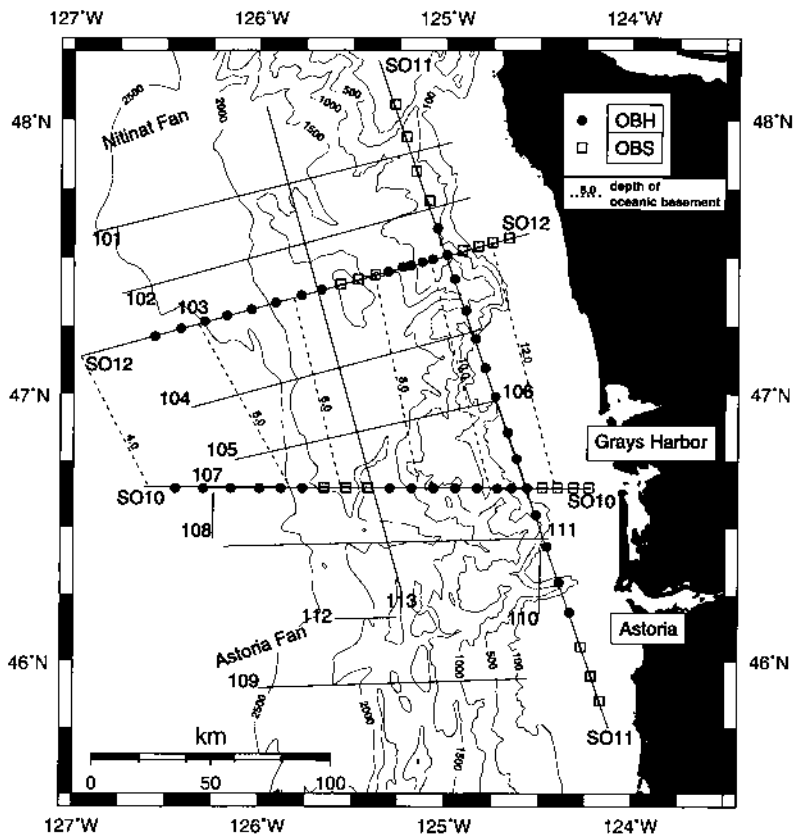


Fig. 2. Location of seismic reflection (101 to 113) and refraction lines (SO10, SO11, and SO12) acquired across the Washington margin during cruise 108 — ORWELL. The depth (km) of oceanic basement is interpolated between the two refraction profiles.

each with eight guns. While collecting wide-angle data, a 104 l (6350 in³) array was deployed and the array volume was reduced to 88 l (5335 in³) for the MCS survey. Onshore portable seismometers, operated by scientists of the USGS and Oregon State University, and permanent earthquake seismometers, operated by the University of Washington, recorded wide-angle data to investigate the deep crustal structure of the continental margin during both offshore wide-angle and MCS data acquisition.

We examined two main areas — one west of central Oregon and the other off Washington. In Fig. 2 a location map of the Washington survey is shown. Line SO10/107 is the westward extension of the 1995 USGS SW-Washington refraction profile (Luetgert et al., 1995), which now extends from the Columbia plateau across the magmatic arc to the Juan de Fuca Plate.

The MCS data have been stacked followed by a constant velocity migration. The western part of two dip lines (those coincident with wide-angle profiles SO10 and SO12) were processed through pre-stack depth migration. All sections reveal the structure of the accretionary wedge in outstanding detail, and when they are combined with velocity information from the wide-angle data, detailed images of the crustal structure across the margin were obtained. In this paper, we present the two MCS profiles off Washington (103 and 107), on which coincident wide-angle data SO10 and SO12) were collected.

2.2. Seismic data analysis

2.2.1. Profile SO12/103

The MCS profile 103 is 170 km long (Fig. 3) and extends from the ocean basin to the shelf. The shot

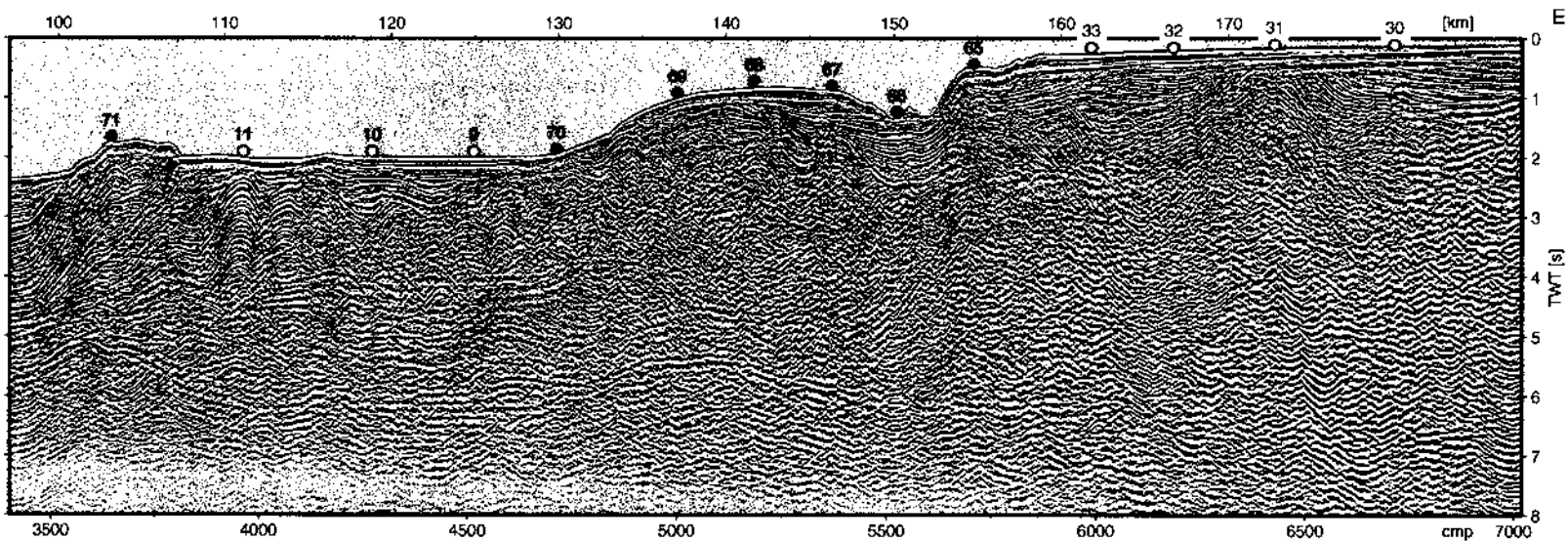
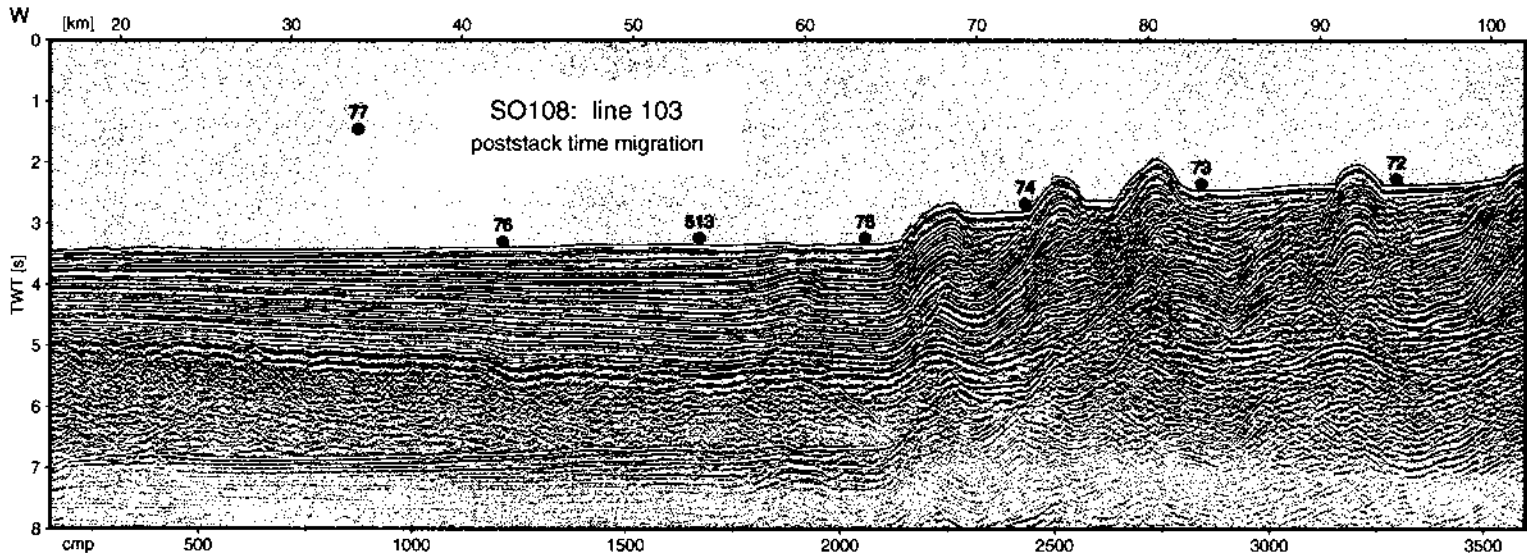


Fig. 3. Post-stack-migration of line 103, vertical exaggeration approx. 5 : 1 at the seafloor.

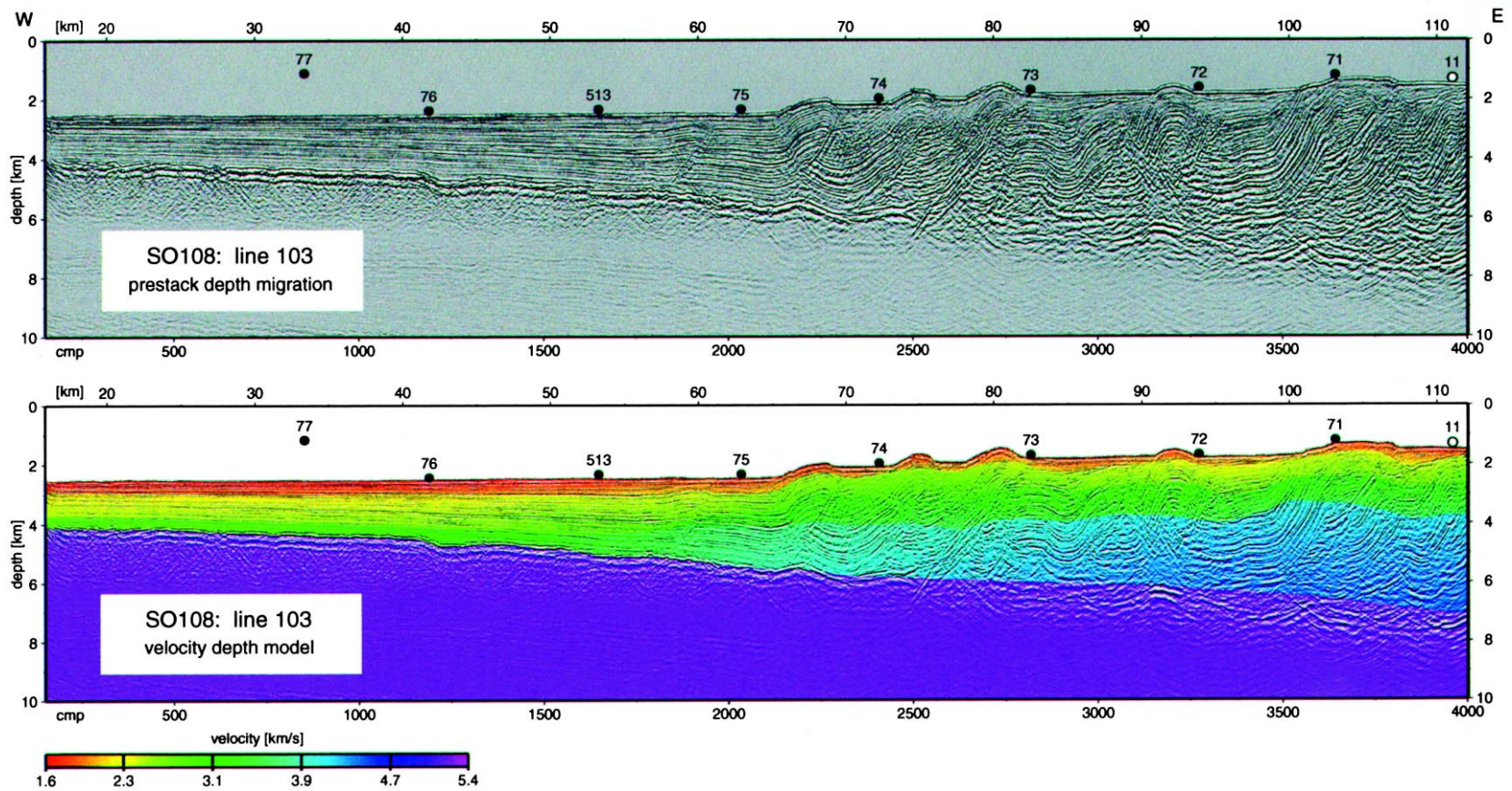


Fig. 4. Pre-stack depth migration of the seaward part of line 103 and velocity model, vertical exaggeration 2 : 1.

spacing was 50 m during the MCS work and 100 m for the wide-angle work. Along this line, a total of 21 OBS were deployed, and all but one recorded useful data. One instrument (OBH 66) was found several miles off its deployment position; it had been dragged by a fishing vessel and recorded the shots about 4 miles off the line. Signals were generally well recorded to distances of 60 km landward and more than 80 km seaward before being overprinted by the water wave from the previous shot. Instruments deployed on the shelf generally show a high noise level, and signal penetration is slightly less than normal. The wide-angle shooting was extended seaward 20 km beyond the end of the MCS line to obtain reversed coverage across the oceanic crust.

Processing of the MCS data was completed to post-stack time migration (Fig. 3) and included a f-k domain multiple suppression process, that is based on move-out differences between primary and multiple events in the CMP gather. To improve the temporal resolution of the seismic data, pre-stack predictive deconvolution was applied followed by a time variant normalization. After CMP stacking, a spatial and time variant application of an f-k filter resulted in the suppression of side-swipe in the data collected on the shelf area. To define the velocity information for time migration, stacking velocities were converted to interval velocities and manually smoothed.

The seaward part of this profile (CMPs 200 to 4000) was further processed using pre-stack depth migration to obtain a more detailed image. The velocity field was established using several iterations of depth focusing error analysis of the MCS data and forward modelling of the OBS recordings using interactive ray-tracing (Luetgert, 1992). The resulting image and the velocity field are shown in Fig. 4 at a vertical exaggeration of 2 : 1. Using all OBS recordings and the post-stack time migration, a structural model for the entire line was achieved as shown in Fig. 5. In the region of overlapping near-vertical and wide-angle coverage, the velocity fields from pre-stack depth migration and from ray-tracing differ by less than ± 0.1 km/s. The velocity field for the pre-stack depth migration is much more detailed and had to be smoothed to avoid artifacts in the ray-tracing. Modelled travel times of the wide-angle data generally fit the observations better than 0.1 s, and in no case differ more than 0.2 s.

2.2.2. Profile SO10/107

Profile SO10 was located between the depocentres of the Nitinat and the Astoria Fans and is 190 km long (Fig. 6). Twenty-one OBS were deployed along this line for the wide-angle experiment. All instruments recorded the airgun shots, but, as for profile SO12, data collected in shallow water suffered from high noise level and poor signal penetration on the upper shelf. Here, the seafloor is formed by a carbonate platform with a rough surface topography exposed by glacial erosion (Flueh and Fisher, 1996). For the nearly 130 km long coincident MCS profile 107, the same processing sequence as for profile 103 was applied. The post-stack migration and the pre-stack depth migration sections with the velocity field are shown in Figs. 6 and 7. The velocity model from the wide-angle data is shown in Fig. 8.

2.3. Data interpretation

2.3.1. Profile SO12/103

On the Juan de Fuca Plate, sediment thickness increases landward towards the margin from 1.5 km to 2.7 km over a distance of 50 km. Three layers can be distinguished by their velocities (Fig. 5). The sediment thickening involves no significant change of water depth and is comprised of the Nitinat Fan deposits. The top of the oceanic crust can be followed throughout the profile and is imaged to a depth of 12 km (Fig. 2) underneath the landwardmost OBS (30), where reflections occur at 6.5 s TWT. The Moho of the Juan de Fuca Plate is clearly recognized from strong wide-angle reflections and Pn phases in the wide-angle data, but is not seen in the MCS data where the corresponding near-vertical reflections are masked by strong multiples.

The velocity within the downgoing oceanic crust was determined from the wide-angle data only, since the focusing error analysis of the pre-stack depth migration has no strong reflections on which to operate and thus little sensitivity at this depth. Correspondingly, first-order velocity discontinuities are absent in the approximately 6 km thick oceanic crust (Fig. 5). The crust can be subdivided into layer 2, layer 3a and 3b, based upon the velocity gradients. Each layer is about 2 km thick, velocities in layer 2 increase rapidly from 4.9 to 6.2 km/s, in layer 3a from 6.2 to 6.8 km/s and from 6.8 to 7.0 km/s in layer 3b.

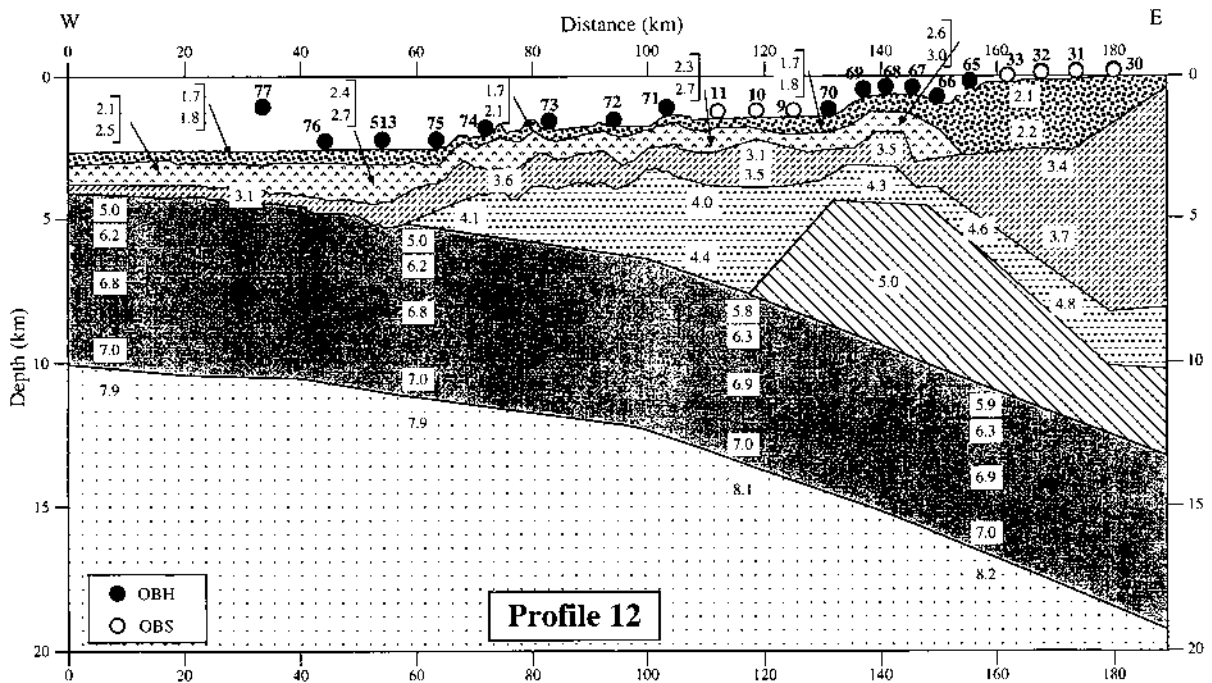


Fig. 5. Velocity model along SO12 from wide-angle data, vertical exaggeration 5 : 1.

Underneath the margin, the velocities in each layer show a moderate increase of about 0.1 to 0.2 km/s when compared to the ocean basin. This increase is most pronounced in layer 2 where the high velocity gradient changes into a moderate velocity gradient at the expense of the low velocities. In the model shown in Fig. 5, the velocities in layer 2 range from 6.0 to 6.2 km/s at the easternmost end. The dip of the oceanic crust increases at the western border of the mid-slope terrace (CMP 2800) from 2° to 4° .

The margin can be subdivided into three units: the lower slope, (CMP 2100 to 3800), the mid-slope terrace (CMP 3800 to 5700) and the shelf (CMP 5700 to 7000) (Fig. 3). Seaward of the lower slope is a 6.5 km wide distributary channel of the Nitinat Fan (CMP 1900 to 2150). Below this channel, a landward vergent thrust fault has developed, and defines the next package of sediment that will be accreted to the toe of the wedge. In this area the wedge consists of six anticlinal thrust faulted ridges, one of which (around CMP 3000) is buried beneath the seafloor. A similar pattern was seen on the profile 101 to the north (Flueh and Fisher, 1996).

2.3.2. Profile SO10/107

The clearly imaged oceanic plate dips 0.5° to 1.5° adjacent to the slope, where sediment is 2.2 km thick. Just landward below the second ridge the dip increases to 3.5° (Fig. 8). Similar to the northern line, the velocities increase from 4.9 km/s on the top (layer 2) to 7.0 km/s at the base of the crust, with no first-order boundary within the oceanic crust. Beneath the middle and upper shelf, velocities in layer 2 increase to 6.0 km/s. Sediment on the incoming Juan de Fuca Plate can be subdivided into three units, with velocities ranging from 1.7 to 2.0 km/s in the first layer, 2.3 to 2.4 km/s in the second and more than 3.0 km/s in the third layer.

Across the shelf, velocities increase rapidly with depth. As for SO12/103, the prism can be subdivided into the lower slope (CMP 3000 to 4300), the mid-slope terrace (CMP 4300 to 1400 and the shelf (CMP <1400) (Fig. 6). The lower slope comprises five ridges. Above the subducting oceanic crust the velocities increase from 4.0 km/s near the toe of the wedge to 5.0 to 5.4 km/s at the end of the profile (Fig. 8). Below the western end of the upper

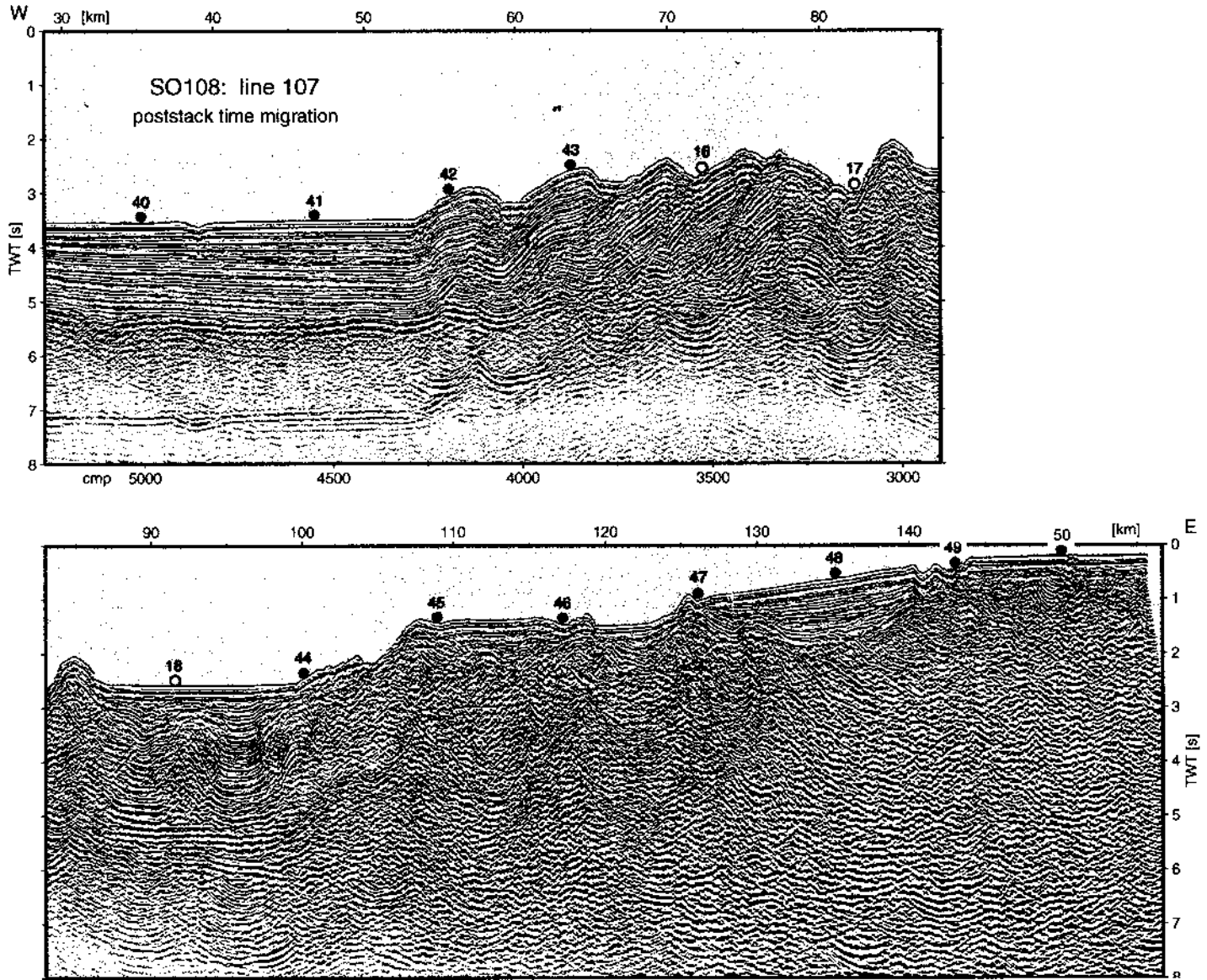


Fig. 6. Post-stack-migration of line 107, vertical exaggeration approx. 5 : 1 at the seafloor.

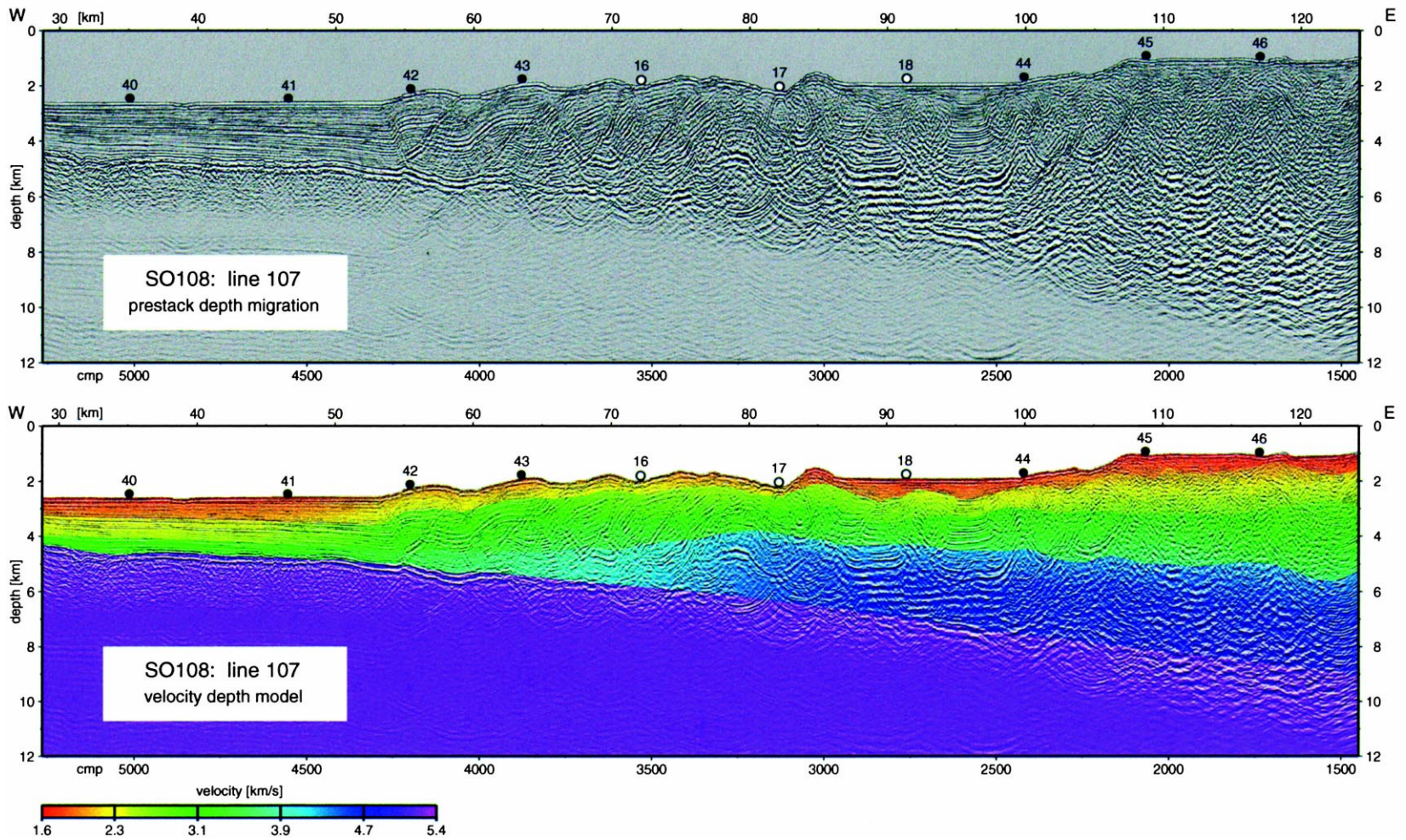


Fig. 7. Pre-stack depth migration of the seaward part of line 107 and velocity model, vertical exaggeration 2 : 1.

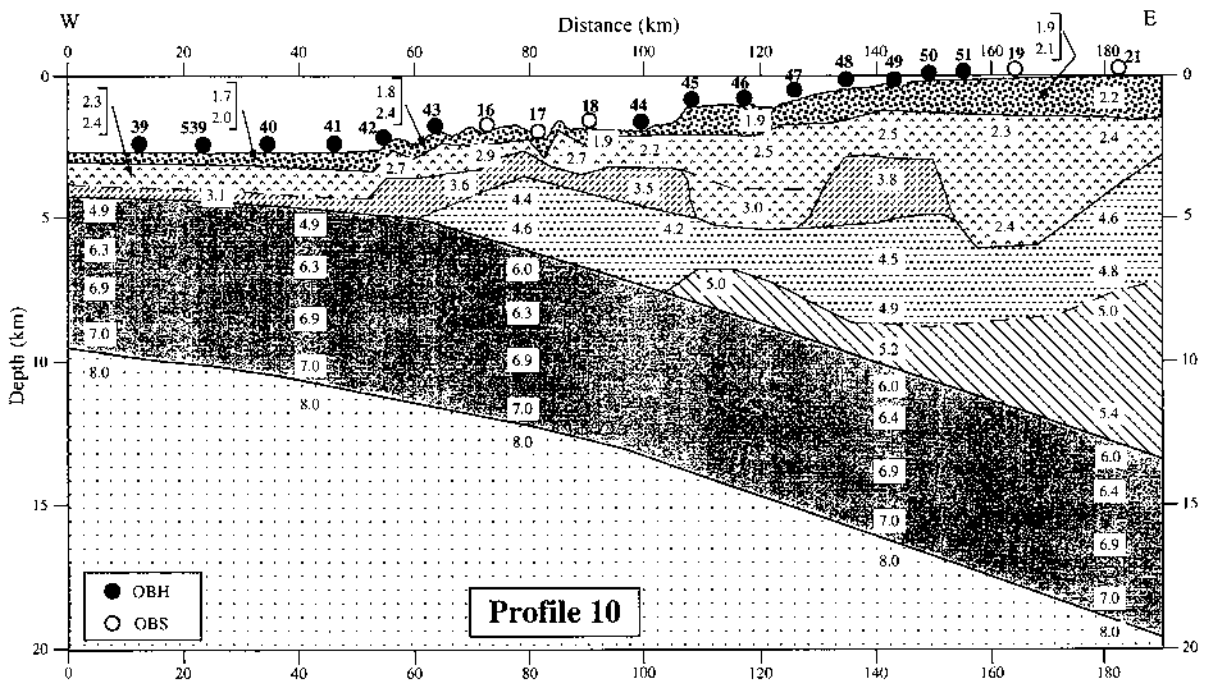


Fig. 8. Velocity model along SO10 from wide-angle data, vertical exaggeration 5 : 1.

shelf, beneath OBS 48 to 50, a high velocity block separates two basins, each about 6 km deep.

3. Discussion

The two lines show a general similarity, but also notable differences. The oceanic plate and its sediment cover is similar on both lines. Near the toe of the wedge, the sediment thickness is 1 km greater on line 103 than on 107 due to the Nitinat Fan. A distinct change in the reflection pattern in the upper plate is seen east of OBH 17 on line 107 and OBH 71 on line 103. To the west, five to six ridges on the seafloor all show a similar deformation pattern with clear landward vergent thrust slices. To the east, the mid-slope terrace is underlain by laterally discontinuous and sharply curved reflections that are covered by undeformed Pleistocene slope deposits with markedly lower velocities. The surface slope angle is approximately 2° on both profiles. At greater depth, reflections of the lower units become discontinuous, except the plate boundary reflection which is imaged to the end of the line.

We tentatively propose that the rocks to the east of where the change in reflection pattern occurs form the backstop for recent accretion. They are from an older period of accretion and are competent enough to have resisted major deformation in the youngest accretionary phase, since reflections near seafloor are essentially undeformed. Deformation at depth may be still occurring here, but does not contradict frontal accretion as demonstrated elsewhere (Kukowski et al., 1994). The area of youngest accretion is 10 km wider (45 km) in line 103 than it is in 107 (35 km). The good control on seismic velocities provides high precision volume estimates. When comparing the two lines we find that within the region of recent accretion an additional cross-sectional area of 70 km² is accommodated along line 103, if 3-D effects are neglected. Taking the sediment thickness at the deformation front as a measure of input (2.2 km for line 107, 2.7 km for line 103), we estimate that the onset of this accretionary phase is roughly 1.5 Ma (Early Pleistocene), assuming uniform convergence rates (4.0 cm/yr), constant sediment input without sediment bypass, and a 20% reduction in the accreted sediment volume due to fluid loss. The largest

uncertainty is the sediment input, since the growth process for Nitinat Fan is difficult to quantify. Interestingly, the volumetric estimates give identical ages for both lines despite the differences in present-day sediment input and volume of the accreted wedge. This, for the first time, clearly documents that the rapid growth of the wedge through landward verging thrusts is a Pleistocene feature, resulting from the high sediment input building the fans, as a consequence of glaciation.

The structural differences in the first ridge document that accretionary structure is laterally at different stages of evolution. The seaward dipping thrust fault that defines the first ridge has a markedly lower slope on 107 than on 103, where it has been rotated to a much steeper angle. The lower dip indicates that this ridge is not yet fully developed and still growing before strain will be transferred seaward to form the next thrust ramp, as on line 103, seaward of the first ridge. The observed structural differences may also be interpreted as reflecting differences in physical properties and the stress regimes. However, since both lines are located on Nitinat Fan no large variations of the physical properties are expected. This is also supported by the similarity of the seismic velocities on both lines (Figs. 5 and 8).

At the first ridge, the depth of the decollement on both lines corresponds to the boundary between the intermediate (2.1–2.5 km/s) and high velocity (3.1 km/s) sedimentary layers, with the high velocity layer bypassing the first ridge. This layer, identified as calcareous pelagic ooze (Duncan and Kulm, 1989), lies between the basement and overlying silt turbidites and interbedded muds. Similar high velocities in this interval have been reported from the Oregon margin (Cochrane et al., 1994), but seem to be absent off Vancouver Island (Yuan et al., 1994). Beginning at the second ridge, the decollement steps down to the oceanic basement and the high velocity layer is offset along a seaward dipping thrust fault, as seen on 103 for the third ridge (CMP 2450–2600). Therefore, the second and third ridges may still be growing.

Five layers can be distinguished in the upper plate in the two velocity models (Figs. 5 and 8). A general velocity gradient is observed landward and downward, and high (>4.0 km/s) velocities are found beneath the toe of the wedge. The velocity increase

begins several kilometres seaward of the deformation front, and was observed elsewhere along the Cascadia margin (Yuan et al., 1994; Cochrane et al., 1994; MacKay, 1995). This observation was interpreted as substantial dewatering, loading-induced physical compaction, and diagenetic changes.

Fragments of igneous crust may account for the high velocities (>5.0 km/s) beneath the shelf. This possibility is supported by the observation that the reflection character of the plate boundary varies in amplitude along the profiles (Figs. 3 and 6). It is not clear whether this variation is an artifact of the acquisition/processing, or indicative of changes in acoustic impedance due to fracturing of the basement as tentatively defined by velocities >5.0 km/s. This is the first well consolidated rock that might store strain energy which could be released during a great earthquake.

Near the edge of the shelf, both profiles display a high velocity (3.5–3.8 km/s) structure at shallow depth, that separates low velocity basins on both sides. Although the incorporation of the land data will later help to define the eastern basins in more detail, the high velocities on profile SO10 are clearly shallower close to the coast. A steeply inclined boundary separating sediment (2.4 km/s) from a 4.6 to 5.4 km/s layer is interpreted as the top of the Siletz Terrane, as suggested by Snively (1987) and also supported by aeromagnetic data (Snively and Wells, 1996). Unfortunately, fishing activity prohibited the collection of MCS data closer to the coast. It is unclear how far the Siletz Terrane extends seaward, since it cannot be distinguished on the basis of velocities alone from rocks underlying the accretionary wedge beneath the mid-slope terrace. In contrast, on profile SO12, rocks with velocities of 5.0 km/s reach as shallow as 5 km beneath the upper slope, with steep boundaries on both sides. Landward, predominantly intermediate velocities are found (3.4 to 3.7 km/s) beneath the Pliocene sediment. This is consistent with earlier suggestions that the Crescent Terrane, the northern continuation of the Siletz Terrane, which is well exposed on the Olympic Peninsula, does not extend offshore on the Washington shelf (Snively and Wagner, 1982), thus no high velocities are expected here. The intermediate velocities probably correspond to the Eocene–Oligocene melange exposed onshore on the Olympic

Peninsula. As for SO10, the nature of the higher velocities (>5.0 km/s) at greater depth remains unknown. Future integration of the land recordings will put further constraints on this region.

4. Conclusions

The two seismic profiles across the accretionary wedge presented here allow the internal tectonic structure and velocity field to be defined in great detail. The dip of the downgoing plate increases towards the continent (Fig. 2), but is significantly shallower than previously assumed (Hyndman and Wang, 1995; Hyndman, 1995). Consequently, a larger part of the plate boundary lies within the cold seismogenic zone. Therefore, the potential area of large earthquakes may extend farther inland and closer to urban areas than previously believed.

The Washington margin accretionary prism is also characterized by a low seafloor dip, which, in combination with the low plate dip, suggests a weak basal decollement. On the other hand, the rapid lateral increase in the velocity argues for a porosity decrease and increasing strength of rocks in the lower part of the accretionary wedge. The coincidence of low basal friction underneath a relatively strong material might be a cause of the seaward verging thrust faults, which is consistent with earlier models (Seely, 1977; MacKay, 1995).

Thrust faults separating ridges at the toe of the prism exhibit a listric shape and, except for the first ridge, extend down to the top of the oceanic basement, indicating that the entire thickness of incoming sediment is frontally accreted. The faults could be efficient pathways for fluid transport. If so, decreased fluid pressure could result temporarily in high basal friction. One could speculate that Cascadia seismicity may exhibit a cyclic behaviour regarding changes in the amount of basal friction. This could be an explanation for the scarcity of seismic events and also for their episodic occurrence (Meyers et al., 1996). However, little is known about the time required to develop high pore pressure regimes in subduction zones (Bekins et al., 1995).

The geometry of the Cascadia subduction zone seems to be much more variable than previously thought, both in space and time. The Washington

margin was strongly influenced by the accretion of Nitinat and Astoria Fan sediment, and thus differs markedly from the Vancouver and central Oregon segments. The onset of glacial sedimentation caused a major reconfiguration of the style of accretion. The two lines presented here from within the Washington margin also show local variability, and we expect, that by balancing these and the remaining lines collected within ORWELL, we shall be able to understand the internal structure and the history of this segment in more detail.

Acknowledgements

The R/V *Sonne* 108 cruise would not have been possible without the support, guidance and encouragement of Roland von Huene of GEOMAR and Steve Bohlen, Craig Weaver, and Ray Wells of the USGS. Special thanks are to Capt. Papenhagen and his crew, who made the cruise so successful. Funding is obtained from the Federal Ministry for Research and Technology (BMBF) of Germany through grant 003G108A and the USGS Hazards programme. We also thank Andrew Calvert and an anonymous reviewer for helpful comments on an earlier draft of this paper.

References

- Applegate, T.B., Goldfinger, C., MacKay, M.E., Kulm, L.D., Fox, C.G., Embley, R.W., Meis, P.J., 1992. A left-lateral strike-slip fault seaward of the central Oregon convergent margin. *Tectonics* 11, 465–477.
- Atwater, B.F., 1992. Geologic evidence for earthquakes during the past 2000 years along the Copalis River, southern coastal Washington. *J. Geophys. Res.* 97, 1901–1919.
- Barnard, W.D., 1978. The Washington continental slope: Quaternary tectonics and sedimentation. *Mar. Geol.* 27, 79–114.
- Bekins, B.A., McCaffrey, A.M., Dreis, S.J., 1995. Episodic and constant flow models for the origin of low-chloride waters in a modern accretionary complex. *Water Resour. Res.* 31, 3205–3215.
- Brandon, M.T., Cowan, D.S., Vance, J.A., 1988. The Late Cretaceous San Juan thrust system. *Geol. Soc. Am. Spec. Pap.* 221, 81 pp.
- Byrne, D.E., Davis, D.M., Sykes, L.R., 1988. Loci and maximum size of thrust earthquakes and the mechanics of the shallow region of the subduction zones. *Tectonics* 7, 833–857.
- Calvert, A.J., 1996. Seismic reflection constraints on imbrication

- and underplating of the northern Cascadia convergent margin. *Can. J. Earth Sci.* 33, 1294–1307.
- Clowes, R.M., Brandon, M.T., Green, A.G., Yorath, C.J., Sutherland Brown, A., Kanasevich, E.R., Spenger, C., 1987. LITHO-PROBE — southern Vancouver Island: Cenozoic subduction complex imaged by deep seismic reflection. *Can. J. Earth Sci.* 24, 31–51.
- Cochrane, G.R., Moore, J.C., MacKay, M.E., Moore, G.F., 1994. Velocity–porosity model of the Oregon accretionary prism from seismic reflection and refraction data. *J. Geophys. Res.* 99, 7033–7043.
- Davis, E.E., Hyndman, R.D., 1989. Accretion and recent deformation of sediments along the northern Cascadia subduction zone. *Geol. Soc. Am. Bull.* 101, 1465–1480.
- Delaney, J.R., Johnson, H.P., Karsten, J.L., 1981. The Juan de Fuca hotspot-propagating rift system: New tectonic, geochemical and magnetic data. *J. Geophys. Res.* 86, 11747–11750.
- DeMets, C., Gordon, R.G., Argus, D.F., Stein, S., 1990. Current plate motions. *Geophys. J. Int.* 101, 425–478.
- Dragert, H., Hyndman, R.D., Rogers, G.C., Wang, K., 1994. Current deformation and the width of the seismogenic zone of the northern Cascadia subduction thrust. *J. Geophys. Res.* 99, 653–668.
- Duncan, R.A., Kulm, L.D., 1989. Plate tectonic evolution of the Cascades arc-subduction complex. *The Geological Society of America, Boulder, CO*, pp. 413–434.
- Engebretson, D.C., Cox, A., Gordon, R.G., 1985. Relative motions between oceanic and continental plates in the Pacific basin. *Geol. Soc. Am. Spec. Pap.* 206, 59 pp.
- Finn, C., 1990. Geophysical constraints on Washington convergent margin structure. *J. Geophys. Res.* 95, 19533–19546.
- Flueh, E.R., Bialas, J., 1996. A digital, high data capacity ocean bottom recorder for seismic investigations. *Int. Underwater Syst. Design* 18 (3), 18–20.
- Flueh, E.R., Fisher, M.A., 1996. FS Sonne Fahrtbericht SO 108 ORWELL, San Francisco, Astoria. *GEOMAR Rep.* 49, 252 pp.
- Heaton, T.H., Kanamori, H., 1984. Seismic potential associated with subduction in the northwestern United States. *Bull. Seismol. Soc. Am.* 74, 933–941.
- Hyndman, R.D., 1995. The Lithoprobe corridor across the Vancouver Island continental margin: the structural and tectonic consequences of subduction. *Geol. Surv. Can.* 31095, 1777–1802.
- Hyndman, R.D., Wang, K., 1993. Thermal constraints on the zone of major thrust earthquake failure: The Cascadia subduction zone. *J. Geophys. Res.* 98, 2039–2060.
- Hyndman, R.D., Wang, K., 1995. The rupture zone of Cascadia great earthquakes from current deformation and the thermal regime. *J. Geophys. Res.* 100, 22133–22154.
- Kukowski, N., von Huene, R., Malavieille, J., Lallemand, S., 1994. Sediment accretion against a buttress beneath the Peruvian continental margin as simulated by sandbox modelling. *Geol. Rundsch.* 83, 1–10.
- Luetgert, J., 1992. Interactive two-dimensional seismic raytracing for the Macintosh. *U.S. Geol. Surv. Open File Rep.* 92-356, 43 pp.
- Luetgert, J., Parsons, T., Miller, K., Keller, G., Trehu, A., Flemming, S., Clowes, R., Asudeh, I., 1995. Crustal architecture of the Pacific Northwest: The 1995 seismic transect across southern Washington (abstr.) *EOS, Trans. Am. Geophys. Union* 76, F399.
- MacKay, M.E., 1995. Structural variation and landward vergence at the toe of the Oregon accretionary prism. *Tectonics* 14, 1309–1320.
- MacKay, M.E., Moore, G.F., Cochrane, G.R., Moore, J.C., Kulm, L.D., 1992. Landward vergence and oblique structural trends in the Oregon margin accretionary prism: Implications and effect on fluid flow. *Earth Planet. Sci. Lett.* 109, 477–491.
- Meyers, R.A., Smith, D.G., Jol, H.M., Peterson, C.D., 1996. Evidence for eight great earthquake-subsidence events detected with ground-penetrating radar, Willapa barrier, Washington. *Geology* 24, 99–102.
- Moore, G.F., Shipley, T.H., Stoffa, P.L., Karig, D.E., Taira, A., Kuramoto, S., Tokuyama, H., Suyehiro, K., 1990. Structure of the Nankai Through accretionary zone from multichannel seismic reflection data. *J. Geophys. Res.* 95, 8753–8765.
- Niem, A.R., Snavely, P.D. Jr., Niem, W.A., 1990. Onshore–offshore geologic cross section from the Mist Gas field, Northern Oregon Coast Range, to the northwest Oregon continental shelf and slope. *Oregon Department of Geology and Mineral Industries Continental Margin Transect OGI-17*, 46 pp., 1 plate.
- Rau, W.W., 1975. Geologic map of the Destruction Island and Taholah quadrangles, Washington. *Washington Division of Geology and Earth Resources, Geologic Map GM-13*, scale 1:62,500.
- Rau, W.W., 1979. Geologic map in the vicinity of the lower Bogachiel and Hoh river valleys, and the Washington coast. *Washington Department of Natural Resources Geologic, Map GM 24*, scale 1:65,000.
- Satake, K., Shimazaki, K., Tsuji, Y., Ueda, K., 1996. Time and size of a giant earthquake in Cascadia inferred from Japanese tsunami records of January, 1700. *Nature* 379, 246–249.
- Seely, D.R., 1977. The significance of landward vergence and oblique structural trends on trench inner slopes. In: Talwani, M. (Ed.), *Island Arcs, Deep Sea Trenches and Back-Arc Basins*. AGU, Washington, DC.
- Sinton, J.M., Detrick, R.S., 1992. Mid-ocean ridge magma chambers. *J. Geophys. Res.* 97, 197–216.
- Snavely Jr., P.D., 1987. Tertiary geologic framework, neotectonics, and petroleum potential of the Oregon–Washington continental margin. In: Scholl, D.S., Grantz, A., Vedder, J.G. (Eds.), *Geology and Resource Potential of the Continental Margin of Western North American and Adjacent Ocean Basins; Beaufort Sea Top Baja California*. Circum-Pac. Council. Energy Miner. Resour. Earth Sci. Ser. 6, 305–335.
- Snavely, P.D. Jr., Kvenvolden, K.A., 1989. Geology and hydrocarbon potential, Preliminary evaluation of the petroleum potential of the Tertiary accretionary terrane, west side of the Olympic Peninsula, Washington (Chapter A). *U.S. Geol. Surv. Bull.* 1892 A-C, 1–17.
- Snavely, P.D. Jr., Wagner, H.C., 1981. Geologic cross section across the continental margin off Cape Flattery, Washington

- and Vancouver Island, British Columbia. U.S. Geol. Surv. Open-File Rep. 81–978.
- Snavely, P.D. Jr., Wagner, H.C., 1982. Geologic cross section across the continental margin of southwestern Washington. U.S. Geol. Surv. Open-File Rep. 82-459, 10 pp.
- Snavely Jr., P.D., Wells, R.E., 1996. Cenozoic evolution of the continental margin of Oregon and Washington. U.S. Geol. Surv. Prof. Pap. 1560, 161–182.
- Snavely, P.D. Jr., Wagner, H.C., Lander, D.L., 1980. Geological cross section of the central Oregon continental margin. Geol. Soc. Am. Map and Chart Ser. MC-28J, scale 1 : 250,000.
- Snavely Jr., P.D., von Huene, R., Miller, J., 1986. Central Oregon margin Line WO756-4. In: von Huene, R. (Ed.), *Seismic Images of Convergent Margin Tectonic Structures*. Am. Assoc. Pet. Geol. Stud. Geol. 25, 24–29.
- Snavely Jr., P.D., von Huene, R., Miller, J., 1987. The central Oregon margin Lines WO76-4. In: von Huene, R. (Ed.), *Seismic Images of Convergent Margin Tectonic Structures*. Am. Assoc. Pet. Geol. Stud. Geol. 26, 24–27.
- Snavely, P.D. Jr., Niem, A.R., MacLeod, N.S., 1989. Geology of the coastal area between Cape Flattery and Cape Alava, northwest Washington. U.S. Geol. Surv. Open-File Rep. 89-141.
- Snavely, P.D. Jr., MacLeod, N.S., Niem, A.R., Minasian, D.L., 1993. Geologic map of Cape Flattery area, northwestern Olympic Peninsula, Washington. U.S. Misc. Invest. Map, 1 : 48,000.
- Tabor, R.W., Cady, W.M., 1978. The structure of the Olympic Mountains, Washington — analysis of a subduction zone. U.S. Geol. Surv. Prof. Pap. 1033, 38 pp.
- Trehu, A.M., Asudeh, I., Brocher, T.M., Luetgert, J.H., Moonery, W.D., Nabelek, J.L., Nakamura, Y., 1994. Crustal architecture of the Cascadia forearc. *Science* 265, 237–243.
- Wang, K., Mulder, T., Rogers, G.C., Hyndman, R.D., 1995. Case for very low coupling stress on the Cascadia subduction fault. *J. Geophys. Res.* 100, 12907–12918.
- Wells, R.E., 1989. Mechanisms of Cenozoic tectonic rotation, Pacific Northwest convergent margin, U.S.A. In: Kissel, C., Laj, C. (Eds.), *Paleomagnetic Rotations and Continental Deformation*. NATO ASI Ser., Kluwer, Dordrecht, pp. 1–16.
- Wells, R.E., 1990. Paleomagnetic rotations and the Cenozoic tectonics of the Cascade arc, Washington, Oregon, and California. *J. Geophys. Res.* 95, 19409–19417.
- Wells, R.E., Heller, P.L., 1988. The relative contribution of accretion, shear, and extension to Cenozoic tectonic rotation in the Pacific Northwest. *Geol. Soc. Am. Bull.* 100, 325–338.
- Wells, R.E., Weaver, C.S., Blakely, R.J., 1996. Crustal block motions in the Pacific Northwest: implications for the earthquake potential of the Cascadia forearc. *Geol. Soc. Am. Abstr. Progr.* 28, 123.
- Yuan, T., Spence, G.D., Hyndman, R.D., 1994. Seismic velocities and porosities in the accretionary wedge sediments at the Cascadia margin. *J. Geophys. Res.* 99, 4413–4427.